POLITECNICO
MILANO 1863

SCUOLA DI INGEGNERIA INDUSTRIALE
E DELL'INFORMAZIONE

Executive Summary of the Thesis

# Nonlinear modeling and control of coaxial rotor UAVs with application to the Mars helicopter

Laurea Magistrale in Space Engineering - Ingegneria spaziale

**Author:** Marcello Sparasci

**Advisor:** Prof. Davide Invernizzi

**Co-advisor:** Prof. Mauro Massari

**Academic year:** 2021/2022

## 1. Introduction

The Red Planet has been on top in the priority list of interplanetary exploration of the solar system. The Mars exploration landers and rovers have laid the foundation of our understanding of the planet atmosphere and terrain. Although the rovers have been a great help, they also have limitations in terms of their speed and exploration capabilities from the ground. Robotic planetary aerial vehicles increase the range of terrain that can be examined, compared to traditional landers and rovers, and have more near-surface capability than orbiters.

The Ingenuity Mars helicopter has been designed by NASA's Jet Propulsion Laboratory to test the technical demonstration of aerial flight in the thin atmosphere of Mars.

A helicopter designed for Mars faces a host of challenging requirements not typically seen on Earth. In this thesis, the most important set of challenges taken under consideration are those related to the flight dynamics of the vehicle when operating in the Martian environment, and how these affect the mechanical design of the vehicle and the flight control algorithms.

Two aspects of the environment are primary drivers for the flight dynamics of a helicopter on Mars:

1. The Martian atmosphere consists primarily of carbon dioxide (CO2) at only 12% of Earth's atmospheric density at sea level, which is equivalent to altitudes around 100.000 ft on Earth.
2. The Martian gravity is approximately 38% of Earth's gravity

Designing a helicopter for Mars also presents serious challenges in terms of testing, verification and validation. It is not possible to fully replicate the Mars environment on Earth; this forces a greater reliance on analysis, modeling and simulation, combined with limited testing in partially replicated environments.

This master thesis focuses on the flight dynamics and control for the Mars Helicopter with the aim of developing a nonlinear dynamic model and a nonlinear control system for position and attitude control relying on data found in the literature about Ingenuity and adapting existing mathematical models of terrestrial coaxial helicopters. The work begins with an overview of Ingenuity design, and ends with the results of numerical simulations carried out in some representative operating conditions using the proposed control design.

## 2. Vehicle overview

The Mars Helicopter design features a coaxial rotor with two counter-rotating hingeless two-bladed rotors measuring 1.21 m in diameter, which are spaced apart by approximately 8% of the rotor diameter [1]. The rotors are designed to operate at speeds up to 2800 rpm. The speed is fixed for the duration of flight, depending primarily on the atmospheric density, which will be in the range of $0.0145-0.0185$ kg/m$^3$. Control of the vehicle motion is achieved using upper and lower swashplates, providing collective control, with a total range of 22° and cyclic control with a range of ±10° for each rotor. Yaw control is achieved using differential collective while keeping the rotor speeds constant via active control of the propulsion motors.

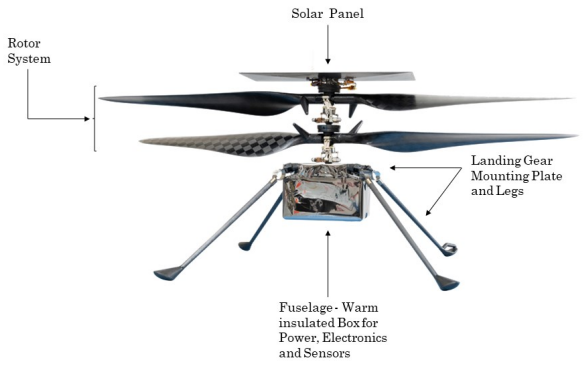


Figure 1: Ingenuity 3D model

The gross vehicle weight is 1.8 kg, a substantial portion of which is taken up by the batteries. The batteries provide energy for flights lasting up to approximately 90 s while also providing sufficient energy for nonflight operation and night-time survival heating. The batteries and other electronics are housed in a cube-like fuselage attached to the central mast, inside of which is a warm electronics box .

The low density Martian atmosphere and the relatively small Mars Helicopter rotors result in very low chord-based Reynolds number flows over a range of $Re_c \approx 10^3$ *to* $10^4$. Furthermore, the low density and low Reynolds number reduce the lifting force and lifting efficiency, respectively, which are only marginally compensated by a lower gravitational acceleration.

All these issues represented a great challenge in the selection of proper airfoil sections for the rotor blades. The blade profile selected is the CLF5605 airfoil designed by Aerovironment. The unusually high first flapping frequency required for stable flight drove the design to a minimum section thickness of the blades. The high first flapping frequency is caused by the low density atmospheric condition affecting the dynamics of blade flapping since the predominant source of damping is aerodynamic. The reduced damping affects the helicopter dynamics in multiple ways, one of which is to introduce poorly damped, oscillatory regressing and advancing flap modes that couple with the body of the helicopter. This is a potential issue for flight control, because a high-bandwidth attitude controller can potentially interact with flap modes destabilizing the system. This issue is solved by making the rotor blades extremely stiff, driving the flap modes to high enough frequencies.

### 2.1. Demonstration vehicle

The vehicle used to demonstrate controlled flight is shown in Fig. 2. It features a full-scale rotor similar to the final vehicle built for Mars flight, but with a slightly larger rotor spacing corresponding to 9% of the rotor diameter. However, because this vehicle was required to lift its own weight in Earth gravity, anything nonessential to the demonstration of controlled flight was left off the vehicle to reduce weight to a total of 765 $g$. Unlike the Mars vehicle, the demonstration vehicle was equipped with cyclic control only on the lower rotor (and collective on both rotors). This provides sufficient degrees of freedom for control but results in reduced control authority and greater cross-axis coupling.

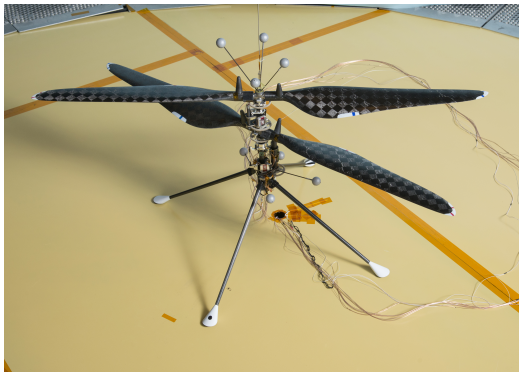

Figure 2: Demonstration vehicle used

## 3. Vehicle dynamics

The configuration of the rigid UAVs can be identified with the motion of a body-fixed frame $F_B = (O_B, \{b_1, b_2, b_3\})$ with respect to a reference frame $F_I = (O_I, \{i_1, i_2, i_3\})$, where $b_j$ and $i_j$ for $j \in \{1, 2, 3\}$ are unit vectors forming right-handed orthogonal triads (with third component pointing down) with $O_B$ located at the center of mass. The dynamic model of the rigid body can be described in body frame by:

$$\begin{cases} m\dot{V}_b + \omega_b \times (mV_b) = F_{ext} & \text{(1a)} \\ I_n\dot{\omega}_b + \omega_b \times (I_n\omega_b) = M_{ext} & \text{(1b)} \end{cases}$$

where $V_b \in R^3$ is the velocity vector in body frame and $\omega_b \in R^3$ is the body-axis angular rates vector; $m$ is the mass of helicopter and $I_n \in R^{3\times3}$ is the inertia tensor; $F_{ext} \in R^3$ and $M_{ext} \in R^3$ are the external forces and moments.

### 3.1. Rotor dynamics

Following the literature on the modeling of small-scale helicopters [5], a simplified model is used to describe rotor dynamics equations
Each rotor of the coaxial helicopter is seen as a rigid disk which can tilt about its longitudinal and lateral axes with angles $a_i$ and $b_i$, respectively, where $i \in \{\text{up}, \text{low}\}$. Their expressions can be derived using the tip-path-plane rotor model and discarding the higher-order terms [5]:

$$\tau_f \dot{b_i} = -b_i - \tau_f p - B_a a_i + B_s B_1 + B_c A_1 \quad \text{(2a)}$$
$$\tau_f \dot{a_i} = -a_i - \tau_f q + A_b b_i - A_s B_1 + A_c A_1 \quad \text{(2b)}$$

In Eq. 2, $A_1$ and $B_1$ are, respectively, the lateral and longitudinal cyclic blade pitch angle defined as functions of the longitudinal and lateral cyclic controls $\delta_{lon}$ and $\delta_{lat}$. $A_b$ and $B_a$ are constants describing the coupling effect between longitudinal and lateral flapping motions. $\tau_f$ is the rotor time constant. Although simple and not reliable for high frequencies, the considered dynamical model is sufficient for the purposes of this work since it allows capturing accurately the low frequency flapping behavior of Ingenuity rotor and the stiff mechanical design places the rotor dynamics far away from the intended control bandwidth.

### 3.2. External forces and moments

The overall contributions to forces and moments acting on the helicopter are:

$$\begin{cases} F_{ext} = F_T + F_g + F_a & \text{(3a)} \\ M_{ext} = M_Q + M_\beta + M_a & \text{(3b)} \end{cases}$$

where $F_T \in R^3$ and $M_Q \in R^3$ are the rotors thrust and torque, respectively; $F_g \in R^3$ is the gravitational force vector in body frame; $M_\beta \in R^3$ is the hub torsional moment vector and $F_a \in R^3$, $M_a \in R^3$ are the aerodynamic forces and moments vectors.

## A. Rotors thrust and torque

According to the aerodynamic actuator disk theory, the magnitude of rotor thrust and rotor moment can be formulated as:

$$T = \rho C_T A \Omega^2 R^2 \quad \text{(4a)}$$
$$Q = \rho C_Q A \Omega^2 R^3 \quad \text{(4b)}$$

where $\rho$ is the air density, $A$ is the rotor disk area, $\Omega$ is the rotor rotational speed, $R$ is the rotor radius, $C_T$ is the rotor thrust coefficient and $C_Q$ is the rotor torque coefficient. All these parameters are constant except for the last two. Since an implementation of a detailed inflow evaluation is not needed for the purposes of this work, an alternative simplified formulation that neglects the radial distribution of the inflow has been taken under consideration. Assuming the blade pitch angle $\theta_i$ and the inflow $\lambda_i$ uniformly distributed along the blade, $C_T$ for both rotors can be computed by:

$$\lambda_i = \frac{C_{T_i}}{2\sqrt{\mu^2 + (\lambda_i - k\lambda_j - \mu_z)^2}} \quad \text{(5a)}$$
$$C_{T_i} = \frac{C_{l_{\alpha,i}}\sigma}{2}\left(\theta_i\left(\frac{1}{3} + \frac{\mu^2}{2}\right) + \frac{\mu_z + k\lambda_j - \lambda_i}{2}\right) \quad \text{(5b)}$$

where $k$ is the coefficient of interaction between rotors (equal to zero for upper rotor).
Similarly, $C_Q$ can be computed using the approximated expression:

$$C_{Q_i} = \lambda_i C_{T_i} + \frac{\sigma}{8} C_{d_i} \quad \text{(6)}$$

where $C_{d_i}$ is the sectional profile drag coefficient.

## B. Aerodynamic forces and moments

Aerodynamics forces and moments act as perturbations of the system due not only of external

wind and body motion but also for the interaction of the flow generated by rotors with the helicopter fuselage.
The aerodynamic forces in the three body directions can be formulated in a quadratic form:

$$F_a = -\frac{\rho}{2} S V_{tot} \|V_{tot}\| \tag{7}$$

where $S \in R^3$ is the effective drag areas vector and $V_{tot} = [V_{ux} V_{vy} V_{wz}]^T$ is the total relative velocity (including wind and propeller induced velocity). Note that the resultant of aerodynamic forces is applied in correspondence of the center of pressure.
On the other hand, the vector of aerodynamic moments vector $M_{aero} \in R^3$ can be defined as:

$$M_a = -\frac{\rho}{2} \begin{bmatrix} A_x C_{lp} V_{ux} p \\ A_y C_{mq} V_{vy} q \\ A_z C_{nr} V_{wz} w \end{bmatrix} + d_{cp} \times F_{aero} \tag{8}$$

where the constants $C_{lp}$, $C_{mq}$ and $C_{nr}$ are the aerodynamic damping moment coefficients.

### 3.3. Nonlinear model

The final model in body frame to be controlled is then:

$$\dot{R} = R\hat{\omega}_b \tag{9a}$$
$$\dot{x} = RV_b \tag{9b}$$
$$m\dot{V}_b + \omega_b \times (mV_b) = F_T + F_g + F_a \tag{9c}$$
$$I_n\dot{\omega}_b + \omega_b \times (I_n\omega_b) = M_Q + M_\beta + M_a \tag{9d}$$
$$\tau_f \dot{b}_i = -b_i - \tau_f p - B_a a_i + B_s B_1 + B_c A_1 \tag{9e}$$
$$\tau_f \dot{a}_i = -a_i - \tau_f q + A_b b_i - A_s B_1 + A_c A_1 \tag{9f}$$

### 3.4. Model tuning

The system in Eq. 9 can be linearized around hovering condition. This has a double goal:

1. Use the linearized dynamics at low frequency in order to evaluate the unknown parameters of the nonlinear model, exploiting the numerical values of Ingenuity's demonstration vehicle stability and control derivatives available [3].
2. Have an adequate model to study the main dynamic characteristics of the system and on which to perform the synthesis of linear control solutions.

The resulting parameterized state-space model can be described in low frequency domain by:

$$M\dot{\bar{x}} = F\bar{x} + G\bar{u} \tag{10}$$

where the linearized flight dynamics is accurately described only by the state vector $\bar{x} = [u; v; w; \Phi; \Theta; \Psi; p; q; r]$: this approximation is acceptable because of the stiff rotor design leading to a rotor dynamics always far from the desired bandwidth of control system. The input vector is defined as $\bar{u} = [\theta_{s0}; \theta_{lc}; \theta_{ls}; \theta_{a0}]$, with $\theta_{s0}$ and $\theta_{a0}$ the symmetric and antisymmetric collective components, respectively. $M \in R^{9\times9}$ is the diagonal inertial matrix, $F \in R^{9\times9}$ is the matrix containing the stability derivatives of the system and $G \in R^{9\times4}$ is the matrix containing the control derivatives of the system.
In order to estimate the stability and control derivatives of the system, it is necessary first to identify the trimming values of the system parameters. In hovering condition, the position of the helicopter is constant and all velocities are set to zero. The flapping motion of blades is null resulting in trimmed cyclic control inputs equal to zero. In hovering, the thrust ratio between rotors can be defined as:

$$\frac{T_{up}}{T_{low}} = 1.4375 \tag{11}$$

which has been derived analytically in [4] for rotors operating in hovering condition at balanced torque with the lower rotor operating in the vena contracta of the upper rotor. The trimmed values of collective control inputs can be identified from Eq. 5 knowing that in hover condition the sum of the thrusts must be equal to the gravitational force.
Once the trimming values of the system, the stability and control derivatives can be evaluated taking the partial derivative of dynamics equations respect to each state and to each control input, respectively. A comparison between Ingenuity identified model reported in [3] and our model has been carried out using the MATLAB function *gapmetric*. The obtained result is a small gap between the two systems implying that any linear controller that stabilizes the Ingenuity identified dynamics system also stabilizes the linearized plant obtained using the proposed modeling technique.
In Fig. 3, the open loop response of roll and pitch torques to steps in the cyclic channels is shown. The response is close to the response of the real system as reported in [3].

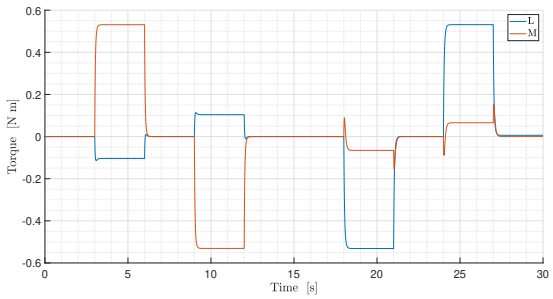


Figure 3: Open loop response of roll and pitch torques to steps in the cyclic channels

## 4. Vehicle control system

The development of the control system starts with the implementation of a linear control system obtained by replicating the architecture proposed in the literature [2] for Ingenuity; this is useful for benchmark purposes and to see the responses of our model to simple commands and its behavior near hovering conditions. After deriving a suitable nonlinear-control oriented model for the Mars Helicopter, a nonlinear control architecture has been designed, which aims at improving the system performance far from hovering and to make the UAV capable of following more complex trajectories.

### 4.1. Baseline controller

Fig. 4 illustrates the overall control architecture implemented in Ingenuity [2], which exploits a cascade architecture to handle the underactuated nature of the helicopter dynamics.
Heave and yaw angle are controlled by a simple PID-type controller. The horizontal position of the vehicle is controlled via a nested architecture. An inner loop is formed by independently controlling roll and pitch with PD-type controllers. The reference input to the inner loop is provided by an outer loop, which is formed by controlling the horizontal position using PID-type controllers. The horizontal position is represented in a local ground frame, whereas the roll and pitch angles are the angles of the body frame relative to gravity direction; therefore, the output of the outer loop is rotated by the yaw angle before being used as a reference by the inner loop.
The first step for the design of control system is the selection of collective and cyclic mixing matrices to decouple control inputs.

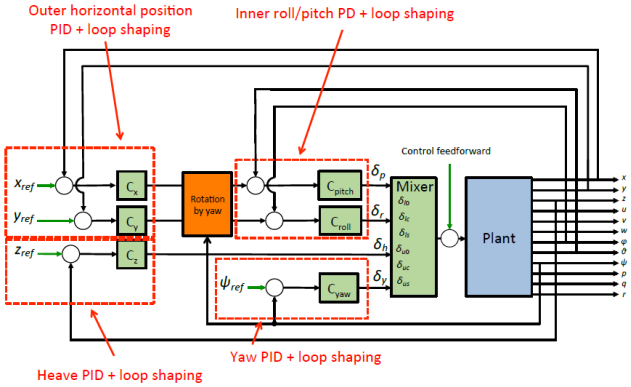


Figure 4: Baseline controller architecture [2]

$M_{col} \in R^{2\times2}$ and $M_{cyc} \in R^{2\times2}$ are taken as inverse matrices such as:

$$\begin{bmatrix}\theta_{s0}\\ \theta_{a0}\end{bmatrix} = \begin{pmatrix} Z_{s0} & Z_{a0} \\ N_{s0} & N_{a0}\end{pmatrix}^{-1} \begin{bmatrix}\delta_h\\ \delta_y\end{bmatrix} \tag{12}$$

$$\begin{bmatrix}\theta_{lc}\\ \theta_{ls}\end{bmatrix} = \begin{pmatrix} L_{lc} & L_{ls} \\ M_{lc} & M_{ls}\end{pmatrix}^{-1} \begin{bmatrix}\delta_r\\ \delta_p\end{bmatrix} \tag{13}$$

where $\delta_h$, $\delta_y$, $\delta_r$ and $\delta_p$ are the control inputs aligned with the respectively axis and the terms inside the matrices are the control derivatives of the linearized system.
The next step is the tuning of PID- and PD-type controllers by considering decoupled dynamics for each axis; they have been tuned taking as plant the linearized model described by Eq. 10 and considering as starting design parameters the stability margins and crossover frequencies reported in [2].
The resulting robustness of the system has been checked through stability analysis with Nichols charts for each channel; then, a multiloop disk margins analysis has been used to quantify the largest complex perturbations that can be injected at the input point to the plant, simultaneously and independently in each channel.
The linear controller has been tested on nonlinear plant through numerical simulations, showing expected results near hovering conditions (Fig. 5), but deteriorated performance far from it (Fig. 6).

### 4.2. Nonlinear controller

The starting point of the nonlinear control design is the development of a simplified nonlinear model that accounts for the main nonlinear effects at small velocities, notably kinematic nonlinearities.

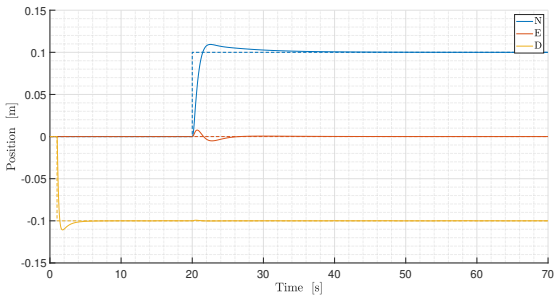


Figure 5: NED position near hovering

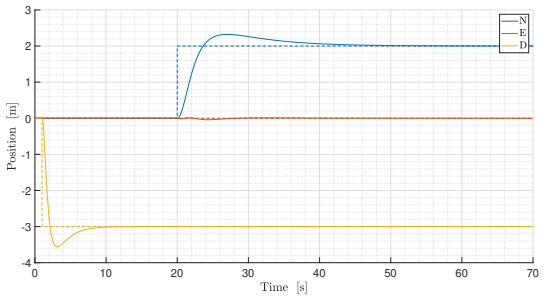


Figure 6: NED position for greater steps

Recalling Eq. 9d, representing it in inertial frame and taking some assumptions, such as steady state rotor dynamics, the resulting mathematical model is described by:

$$\begin{cases} \dot{x} = v & \text{(14a)} \\ m\dot{v} = -mge_3 + T_c R e_3 + \tilde{f}_e & \text{(14b)} \\ \dot{R} = R\hat{\omega}_b & \text{(14c)} \\ J\dot{\omega}_b = -\hat{\omega}_b J\omega_b + \tau_c + \tau_e & \text{(14d)} \end{cases}$$

where $v \in R^3$ is the inertial translational velocity, $T_c$ and $\tau_c \in R^3$ are are the overall thrust and the torque applied by the propellers, respectively, and $(\tilde{f}_e, \tau_e) \in R^3$ collects all disturbance terms.
The allocation matrix of the system is defined by:

$$\begin{bmatrix} \theta_{s0} \\ \theta_{a0} \\ \theta_{lc} \\ \theta_{ls} \end{bmatrix} = \begin{pmatrix} M_{col}^{-1} & \\ & M_{cyc}^{-1} \end{pmatrix} \begin{bmatrix} T_c \\ L_c \\ M_c \\ N_c \end{bmatrix} \quad (15)$$

A nonlinear cascaded controller for position-yaw setpoint regulation has been implemented to tackle the platform underactuation; the control architecture corresponds to a double cascade P/PID nonlinear controllers for position and attitude control with a planner in the middle (see Fig. 7)

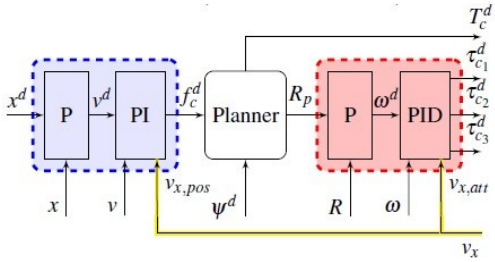


Figure 7: Nonlinear controller architecture

The control law is described by:

$$f_c^d = sat(PI_x(s)(k_{p,x}^0(x - x^d) - v)) + mge_3$$

$$\begin{cases} T_c^d = ||f_c^d||, \quad b_{p_3} = \frac{f_c^d}{||f_c^d||} \\ R_p = \left[ \frac{b_{p_3} \times b_{d_1}}{||b_{p_3} \times b_{d_1}||} \times b_{p_3} \quad \frac{b_{p_3} \times b_{d_1}}{||b_{p_3} \times b_{d_1}||} \quad b_{p_3} \right] \end{cases}$$

$$\tau_c^d = PI_R(s)(\omega^d(K_{p,R}(R_p^T R) - \omega) - D_R(s)\omega$$

where $PI_{(.)}(s)$ and $D_{(.)}(s)$ are continuos functions defining, respectively, a proportional integral and derivative actions. The rotation matrix $R_p \in SO(3)$ is the reference signal to be tracked by the attitude controller and $\omega_d$ is a nonlinear proportional stabilizer assigning the reference velocity to the inner-loop attitude PID controller:

$$\omega^d(K_{p,R}R_p^T R) = 2K_{p,R}sgn(q_e(R_p))\mathbf{q}_e(R_p)$$

where $q_e(R_p) \in R$ and $\mathbf{q}_e(R_p) \in R$ are the vectorial and the scalar part of the quaternion error $q_e \in S^3$. A *back calculation* anti-windup method has been introduced in order to manage the saturation of the PI and not ruin the performances of the controller. The proposed position control law can be interpreted as a conditional integrator [6], a control design that combines the behavior of a sliding mode controller, a powerful solution to handle large exogenous disturbances that would make the actuator saturate, and of a PI controller for small errors, which can be tuned to a achieve desired level of performance with linear design tools.
Thanks to the structure of the proposed control law, a linearized version of the closed-loop system could be used to carry out tuning of the gains so that the controller achieves the same performance requirements identified for the baseline but also global stability results on the nonlinear control model.
The nonlinear control law has been tested trough

different numerical simulations: first, near hovering conditions and then far from the design point. The results obtained show the same performances of the baseline controller near equilibrium, with a better decoupling between axis, and a good response of the system to great step inputs (Fig. 8) and to follow complex trajectories like the one illustrated in Fig. 9, where the UAV after reaching an altitude of 3 m performs lateral and longitudinal translations of 20 m and 10 m, respectively, before returning to the initial point. Note that a three-second horizontal gust of magnitude 10 m/s is applied at time $t = 42$ s; in Fig. 10, the peak of displacement along the x axis due to wind is visible, but its magnitude is low showing the robustness of the designed control law even in the presence of external disturbances. In order to show the differences between nonlinear controller and baseline controller, the same maneuver has been carried out using the linear controller (Figs .11 and 12).

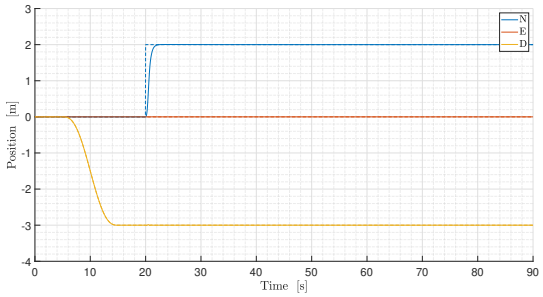


Figure 8: NED position for great steps

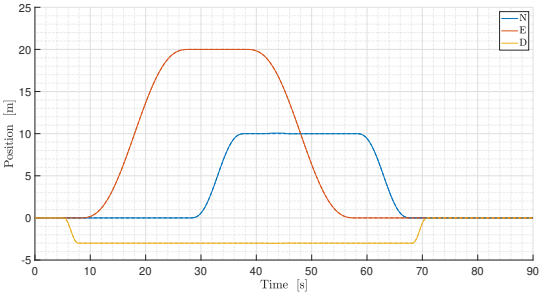


Figure 9: NED position for complex trajectory with wind

## 5. Conclusions

In the presented thesis, a nonlinear dynamic model of the Mars helicopter has been derived for simulation purposes and for the preliminary

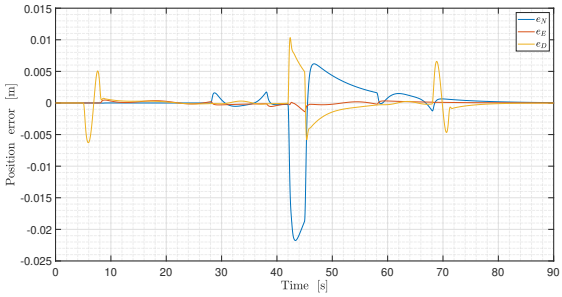


Figure 10: Tracking error of NED position for complex trajectory with wind

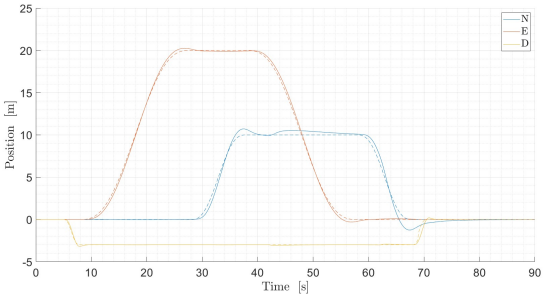


Figure 11: NED position for complex trajectory with wind and using linear controller

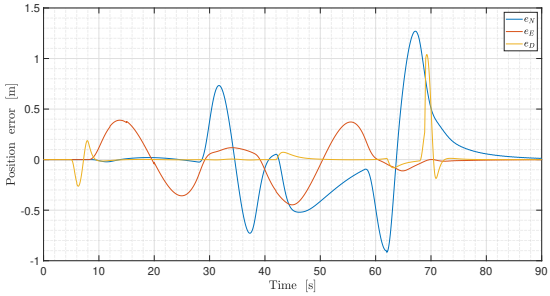


Figure 12: Tracking error of NED position for complex trajectory with wind and using linear controller

derivation and validation of nonlinear control laws.

While simple, the parameters of the nonlinear model could be tuned to achieve a behavior very similar to the demonstrator vehicle of the Mars Helicopter in near hovering conditions, by exploiting identification experiments reported in the literature.

In the second part of the thesis, the control system has been developed starting with the implementation of a linear controller obtained by replicating the architecture proposed in literature for Ingenuity and following with

the development of the proposed nonlinear controller. Both controllers have been tuned properly checking their performances through linear stability analysis as Nichols charts and MIMO disk margins.
The numerical simulations carried out have shown good results of the baseline controller when the system operates near hovering condition, but deteriorated performance far from it. The implementation of a nonlinear control law has improved the system performance far from hovering and has made the UAV capable of following more complex trajectories.

## References

[1] Bob Balaram, Timothy Canham, Courtney Duncan, Håvard F Grip, Wayne Johnson, Justin Maki, Amelia Quon, Ryan Stern, and David Zhu. Mars helicopter technology demonstrator. In *2018 AIAA Atmospheric Flight Mechanics Conference*, page 0023, 2018.

[2] Håvard F Grip, Daniel P Scharf, Carlos Malpica, Wayne Johnson, Milan Mandic, Gurkirpal Singh, and Larry A Young. Guidance and control for a mars helicopter. In *2018 AIAA Guidance, Navigation, and Control Conference*, page 1849, 2018.

[3] Håvard Fjær Grip, Wayne Johnson, Carlos Malpica, Daniel P Scharf, Milan Mandić, Larry Young, Brian Allan, Bérénice Mettler, Miguel San Martin, and Johnny Lam. Modeling and identification of hover flight dynamics for nasa's mars helicopter. *Journal of Guidance, Control, and Dynamics*, 43(2):179–194, 2020.

[4] Monica Syal J. Gordon Leishman. Figure of Merit Definition for Coaxial Rotors. *Alfred Gessow Rotorcraft Center, Department of Aerospace Engineering Glenn L. Martin Institute of Technology University of Maryland, College Park, MD*, July 2008.

[5] Bernard Mettler. *Identification modeling and characteristics of miniature rotorcraft*. Springer Science & Business Media, 2013.

[6] Sridhar Seshagiri and Hassan K Khalil. Robust output feedback regulation of minimum-phase nonlinear systems using conditional integrators. *Automatica*, 41(1):43–54, 2005.